Oxidative Scission of a Mo−Mo Quadruple Bond

F. Albert Cotton,*,† Carlos A. Murillo,*,†,‡ and Hong-Cai Zhou†

The Laboratory for Molecular Structure and Bonding, Department of Chemistry, P.O. Box 30012, Texas A&M University, College Station, Texas 77842-3012, and Department of Chemistry, Universidad de Costa Rica, Ciudad Universitaria, Costa Rica

Received January 28, 2000

Two compounds containing the cations $Mo_2(DPhIP)_4^{n+}$, $n = 1$ or 2 and DPhIP = the anion of 2,6-diphenyliminopiperidine, have been obtained by oxidation of the quadruply-bonded $Mo_2(DPhIP)_4$ species. The first oxidation process conserves the structure but results in a slight increase of the Mo−Mo distance from 2.114(1) to 2.136(2) Å in $[Mo_2(DPhIP)_4](PF_6)\cdot 2CH_2Cl_2$ (**1**·$2CH_2Cl_2$). However, the second oxidation process breaks the dimolybdenum bond, giving a bioctahedral complex, $[Mo_2(DPhIP)_4](BF_4)_2\cdot 5CH_3CN\cdot Et_2O$ (**2**·$5CH_3CN\cdot Et_2O$), with Mo···Mo separation of 2.9954(7) Å. Crystallographic data for **1**·$2CH_2Cl_2$ are space group $C2/c$, $a = 17.1891(9)$ Å, $b = 17.807(1)$ Å, $c = 24.210(2)$ Å, $\beta = 106.403(4)°$, $Z = 4$; for **2**·$5CH_3CN\cdot Et_2O$, space group $P2_1/n$, $a = 16.523(5)$ Å, $b = 27.418(5)$ Å, $c = 18.163(3)$ Å, $\beta = 93.48(2)°$, $Z = 4$.

Introduction

The oxidation of paddlewheel complexes of the Mo_2^{4+} unit has been studied previously, but not very extensively. There is no report of the isolation of any compound containing a $Mo_2(O_2CCH_3)_4^+$ ion, although from a photoelectron spectroscopic study[1] of $Mo_2(O_2CR)_4$ in the vapor phase we know that the removal of one δ electron causes an increase in the Mo−Mo distance[2] and a reduction in the Mo−Mo stretching frequency from 406 to 360 cm^{-1}.

Paddlewheel molecules in which the bridging ligands employ two nitrogen atoms to bind to the metal atoms have allowed the preparation of several cationic species. It was shown in 1989[3] that $Mo_2(DTolF)_4$[4] can be oxidized to afford $[Mo_2(DTolF)_4]PF_6$, with the Mo−Mo bond distance increasing from 2.085(4) to 2.122(3) Å. The compound $Mo_2(DTolF)_4$ can also be oxidized by $[Cp_2Fe]Cl$ to $Mo_2(DTolF)_3Cl_2$, where a Mo−Mo distance of 2.1510(5) has been reported.[5] Similarly, $Mo_2[(PhN)_2CNHPh]_4$ can be oxidized[6] to afford $\{Mo_2[(PhN)_2CNHPh]_4\}BF_4$ with an increase of the bond length from 2.084(1) to 2.121(1) Å.[7]

Finally, in 1997, for the first time, a compound containing a paddlewheel with an Mo_2^{6+} core was reported.[7] The Mo−Mo distance here, $[Mo_2(hpp)_4](BF_4)_2$, is 2.142(2) Å compared to 2.067(1) Å in $Mo_2(hpp)_4$. The intermediate oxidation state, $[Mo_2(hpp)_4]Cl$, has a Mo−Mo distance of 2.128(2) Å.[8] In $[Mo_2(hpp)_4](BF_4)_2$, one fluorine atom of each BF_4^- anion is aligned along the Mo−Mo vector and sits 2.768(6) Å away.[7] In $[Mo_2(hpp)_4]Cl$, the molecules line up as a Mo−Mo···Cl···Mo−Mo extended structure. The axial Cl ion is 3.090(6) and 3.314(6) Å away from neighboring Mo atoms.[8] In either case, no significant axial coordination was found.

In this paper we present the novel behavior of another paddlewheel complex of Mo_2^{4+} upon oxidation. In this case, the result of the first step was as expected, but in the second step an unforeseen but understandable result was obtained. Examples of structures relevant to those of the second step presented here are a series of so-called ESBO (edge-sharing bioctahedral) complexes,[9] where two μ-Cl^- anions or two μ,η^1-O_2CR^- groups were found to be sharing an edge of two octahedrally coordinated dimolybdenum units; although the Mo−Mo bonds were lengthened significantly, they were not broken completely.

Experimental Section

All syntheses and manipulations were carried out under an atmosphere of nitrogen with standard Schlenk and glovebox techniques. The compound $Mo_2(DPhIP)_4$ was synthesized according to a literature method,[10] while $AgPF_6$ and $(NO)BF_4$ were purchased from Strem Chemicals. All solvents were freshly distilled over suitable drying reagents under N_2.

Preparation of $[Mo_2(DPhIP)_4](PF_6)\cdot 2CH_2Cl_2$, $1\cdot 2CH_2Cl_2$. The red crystalline solid of $Mo_2(DPhIP)_4$ (0.29 g, 0.25 mmol) was dissolved in CH_2Cl_2 (10 mL); a dark red solution was obtained. A solution of $AgPF_6$ (0.063 g, 0.25 mmol) in CH_2Cl_2 (5 mL) was then added slowly. A dark brown suspension was obtained immediately. After the reaction mixture was stirred at room temperature for 1 h, a filtration was performed with the aid of Celite. The dark brown filtrate was then layered with hexanes. A golden microcrystalline solid, **1**·$2CH_2Cl_2$, was obtained after a week. Yield: 0.25 g, 64%. IR (KBr pellet, cm^{-1}): 1699

† Texas A&M University.
‡ Universidad de Costa Rica.

(1) Lichtenberger, D. L.; Blevins, C. H. *J. Am. Chem. Soc.* **1984**, *106*, 1636.
(2) Miskowski, V. M.; Brinza, D. E. *J. Am. Chem. Soc.* **1989**, *111*, 4244.
(3) Cotton, F. A.; Feng, X.; Matusz, M. *Inorg. Chem.* **1989**, *28*, 594.
(4) Abbreviations used: DTolF = anion of *N*,*N*′-di-*p*-tolylformamidine; hpp = anion of 1,3,4,6,7,8-hexahydro-2*H*-pyrimido[1,2-*a*]pyrimidine; DPhIP = anion of 2,6-di(phenylimino)piperidine.
(5) Cotton, F. A.; Jordan, G. T., IV; Murillo, C. A.; Su, J. *Polyhedron* **1997**, *16*, 1831.
(6) Bailey, P. J.; Bone, S. F.; Mitchell, L. A.; Parsons, S.; Taylor, K. J.; Yellowlees, L. J. *Inorg. Chem.* **1997**, *36*, 867, 5420.
(7) (a) Cotton, F. A.; Daniels, L. M.; Murillo, C. A.; Timmons, D. J. *Chem. Commun.* **1997**, 1499.
(8) Timmons, D. J. Ph.D. Dissertation, Texas A&M University, May 1999.
(9) (a) Cotton, F. A.; Su, J.; Yao, Z. *Inorg. Chim. Acta* **1997**, *266*, 65. (b) Su, J. Ph.D. Dissertation, Texas A&M University, May 1996.
(10) Cotton, F. A.; Murillo, C. A.; Roy, L. E.; Zhou, H.-C. *Inorg. Chem.*, **2000**, *39*, 1743.

10.1021/ic000092t CCC: $19.00
Published on Web 06/23/2000

Table 1. Crystal Data and Structure Refinement

	1·2CH_2Cl_2	**2**·5CH_3CN·Et_2O
chem formula	$C_{70}H_{68}N_{12}Cl_4F_6PMo_2$	$C_{82}H_{89}N_{17}OB_2F_8Mo_2$
fw	1556.01	1694.20
space group	*C*2/*c*	$P2_1/n$
a, Å	17.1891(9)	16.523(5)
b, Å	17.807(1)	27.418(5)
c, Å	24.210(2)	18.163(3)
α, deg	90	90
β, deg	106.403(4)	93.48(2)
γ, deg	90	90
V, Å^3	7108.8(7)	8213(3)
Z	4	4
data collection	Nonius FAST	Nonius FAST
T, K	213(2)	213(2)
radiation *λ*, Å	0.71073	0.71073
ρ(calcd), g cm^{-3}	1.454	1.370
μ(Mo Kα), cm^{-1}	9.13	3.79
R1[a,c]/R1[a,d]	0.086/0.105	0.054/0.063
wR2[b,c]/wR2[b,d]	0.207/0.234	0.131/0.147

[a] $R1 = \sum(|F_o| - |F_c|)/\sum|F_o|$. [b] $wR2 = [\sum[w(F_o^2 - F_c^2)^2]/\sum[w(F_o^2)^2]]^{1/2}$; $w = 1/[\sigma^2(F_o^2) + (aP)^2 + bP]$, $P = [\max(F_o^2 \text{ or } 0) + 2(F_c^2)]/3$. [c] Denotes value of the residual considering only the reflections with $I > 2\sigma(I)$. [d] Denotes value of the residual considering all the reflections.

Table 2. Selected Bond Lengths (Å) and Bond Angles (deg) for **1**

Mo(1)−Mo(1)#1[a]	2.136(2)	Mo(1)−N(31)#1	2.171(7)
Mo(1)−N(11)#1	2.159(7)	Mo(1)−N(32)	2.131(6)
Mo(1)−N(12)	2.132(7)		

N(12)−Mo(1)−Mo(1)#1	90.7(2)
N(32)−Mo(1)−Mo(1)#1	91.2(2)
Mo(1)#1−Mo(1)−N(11)#1	92.5(2)
Mo(1)#1−Mo(1)−N(31)#1	92.2(2)

[a] Symmetry transformation used to generate equivalent atoms: #1 $-x, y, -z + {}^1/_2$.

Table 3. Selected Bond Lengths (Å) and Angles (deg) for **2**

Mo(1)−Mo(2)	2.9954(7)	N(32)−Mo(1)−N(21)	87.4(2)
Mo(1)−N(12)	2.158(4)	N(32)−Mo(1)−N(12)	142.8(2)
Mo(1)−N(13)	2.209(4)	N(21)−Mo(1)−N(12)	90.5(2)
Mo(1)−N(21)	2.157(4)	N(32)−Mo(1)−N(41)	92.3(2)
Mo(1)−N(32)	2.152(4)	N(21)−Mo(1)−N(41)	175.5(2)
Mo(1)−N(33)	2.212(4)	N(12)−Mo(1)−N(41)	87.0(2)
Mo(1)−N(41)	2.170(4)	N(32)−Mo(1)−N(13)	157.2(4)
Mo(2)−N(11)	2.169(4)	N(21)−Mo(1)−N(13)	88.9(2)
Mo(2)−N(22)	2.158(4)	N(12)−Mo(1)−N(13)	59.7(2)
Mo(2)−N(23)	2.207(4)	N(41)−Mo(1)−N(13)	93.0(2)
Mo(2)−N(31)	2.159(4)	N(32)−Mo(1)−N(33)	59.7(2)
Mo(2)−N(42)	2.150(4)	N(21)−Mo(1)−N(33)	93.4(2)
Mo(2)−N(43)	2.207(4)	N(12)−Mo(1)−N(33)	157.4(2)
		N(41)−Mo(1)−N(33)	90.3(2)
		N(13)−Mo(1)−N(33)	98.1(2)

(w), 1684 (w), 1648 (m), 1595 (w), 1558 (sh), 1529 (vs), 1451 (s), 1417 (m), 1370 (m), 1262 (w), 1224 (m), 1192 (m), 1075 (w), 1029 (w), 976 (w), 842 (vs), 800 (w), 765 (w), 716 (w), 698 (w), 558 (w), 508 (w), 420 (w). UV/vis (CH_2Cl_2): 391 nm (sh, ϵ = ca. 6700 cm^{-1} mol^{-1} L), 446 (sh, 2450), 651 (490). Dark brown block-shaped crystals suitable for crystallographic studies were grown by diffusion of hexanes into a dilute CH_2Cl_2 solution of **1** at −10 °C for 2 weeks. Anal. for **1**·2CH_2Cl_2. Found: C, 53.29; H, 4.33; N, 10.36. Calcd: C, 54.03; H, 4.40; N, 10.80.

Preparation of $Mo_2(DPhIP)_4(BF_4)_2$·5CH_3CN·Et_2O, 2·5CH_3CN·Et_2O. To a dark red solution of $Mo_2(DPhIP)_4$ (0.288 g, 0.25 mmol) in CH_2Cl_2 (15 mL) was added $NOBF_4$ (0.09 g, 0.5 mmol). A dark brown suspension was obtained. After stirring overnight, the suspension was mixed with hexanes, which resulted in the precipitation of a dark powder in quantitative yield. Prismatic, dark-brown crystals of X-ray quality were obtained from an CH_3CN solution of **2** layered with diethyl ether which was kept at −20 °C for 10 days. IR (KBr pellet, cm^{-1}): 1636

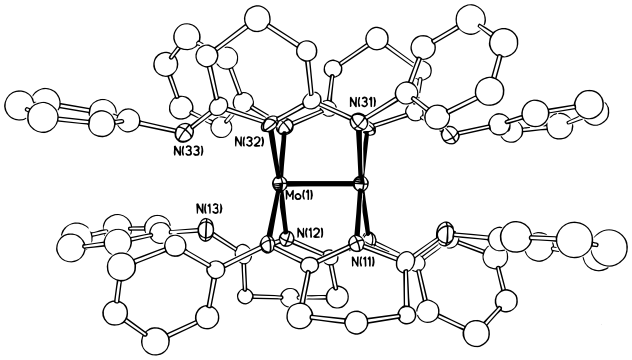

Figure 1. The structure of the $[Mo_2(DPhIP)_4]^+$ cation. Only one orientation of the disordered part is shown. Displacement ellipsoids are shown at the 30% probability level; hydrogen atoms are omitted for clarity.

(w), 1617 (w), 1596 (w), 1577 (w), 1558 (m), 1529 (vs), 1509 (m), 1490 (m), 1473 (m), 1451 (vs), 1415 (s), 1372 (s), 1330 (w), 1262 (m), 1226 (s), 1193 (s), 1156 (w), 1072 (vs), 1050 (vs), 976 (w), 937 (w), 916 (w), 865 (m), 800 (s), 762 (m), 717 (s), 696 (s), 678 (w), 634 (w), 607 (w), 508 (m), 472 (w), 458 (w), 419 (m). UV/vis (CH_2Cl_2): 428 nm (sh, ϵ = ca. 3360 cm^{-1} mol^{-1} L), 555 (310), 650 (508), 772 (50). Mass spectrometry (FAB+, NBA as matrix, *m*/*z*): 1240, $[Mo_2(DPhIP)_4]^+$; 976, $[Mo_2(DPhIP)_3]^+$. Anal. for **2**. Found: C, 56.85; H, 4.35; N, 11.37. Calcd: C, 57.73; H, 4.56; N, 11.88.

Physical Measurements. The UV/visible spectra were measured on a Cary 17D spectrometer at ambient temperature using a quartz cell (800−280 nm). Infrared data were recorded on KBr pellets using a Perkin-Elmer 16 PC FT-IR spectrometer. Cyclic voltammetry measurements were carried out on a BAS 100 electrochemical analyzer in 0.2 M $(Bu^n)_4NBF_4$ solution in CH_2Cl_2 with a Pt working electrode and a Ag/AgCl reference electrode; ferrocene was oxidized at 650 mV under the experimental conditions. NMR spectra were recorded on a Varian VXR-300 spectrometer. Elemental analyses were performed by Canadian Microanalytical Services Ltd.

Crystallographic Studies

All data collection was carried out on a Nonius FAST area detector diffractometer with each crystal mounted on the tip of a glass fiber under a stream of nitrogen at −60 °C. Cell parameters were obtained by least-squares refinement of 250 reflections ranging in 2θ from 18.1° to 41.6°. Laue groups and centering conditions were confirmed by axial images. Data were collected using 0.2° intervals in φ over the range $0° \le \varphi \le 220°$ and 0.2° intervals in ω for two different regions in the range $0° \le \omega \le 72°$; in this way, nearly a full sphere of data was collected. The highly redundant data sets were corrected for Lorentz and polarization effects and for absorption.

The positions of the metal atoms and some of the atoms of the first coordination sphere were located from direct-methods *E*-maps; other non-hydrogen atoms were found in alternating difference Fourier syntheses and least-squares refinement cycles and, during the final cycles, refined anisotropically. Hydrogen atoms were placed in calculated positions.

In compound **1**·2CH_2Cl_2, all the phenyl rings and piperidyl rings were found to be disordered. They were modeled as having two or three orientations; the occupancy of each orientation was optimized with SHELXL. In compound **2**·5CH_3CN·Et_2O, the interstitial solvent molecules were also disordered; they were modeled as a superposition of two orientations with approximately half occupancy for each orientation.

Crystallographic data for **1**·2CH_2Cl_2 and **2**·5CH_3CN·Et_2O are given in Table 1; selected bond distances and angles for **1**·2CH_2Cl_2 and **2**·5CH_3CN·Et_2O are listed in Tables 2 and 3, respec-

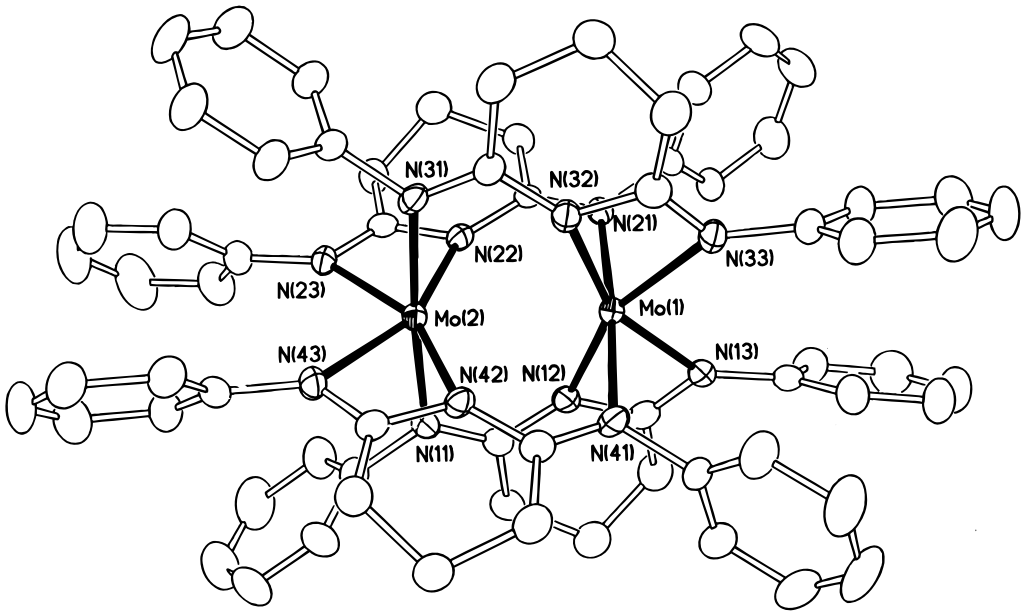

Figure 2. The $[Mo_2(DPhIP)_4]^{2+}$ cation. Displacement ellipsoids are drawn at the 50% probability level; hydrogen atoms are omitted for clarity.

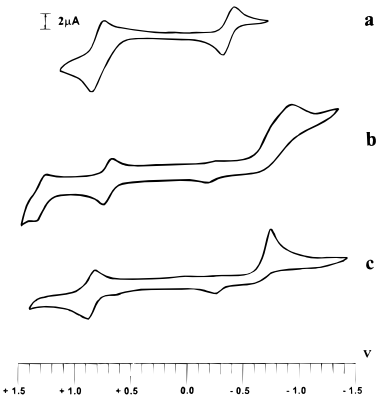

Figure 3. Cyclic voltammograms of (from top to bottom) $Mo_2(DPhIP)_4$, $[Mo_2(DPhIP)_4](PF_6)$, **1**, and $[Mo_2(DPhIP)_4](BF_4)_2$, **2**.

tively. The structures of the cations of compounds **1** and **2** are given in Figures 1 and 2, respectively.

Results and Discussion

As shown by its cyclic voltammogram illustrated in Figure 3a, $Mo_2(DPhIP)_4$, DPhIP = the anion of 2,6-diphenyliminopiperidine, shows a reversible and a quasi-reversible oxidation at $E_{1/2}$ values of −338 and 820 mV, respectively, suggesting that the oxidation states Mo_2^{5+} and Mo_2^{6+} are accessible. Since the formal potential of Ag^+/Ag in CH_2Cl_2 is 1300 mV[11] (vs Ag/AgCl), which is higher than the second oxidation potential shown in Figure 3a, the CH_2Cl_2 solution of $AgPF_6$ needs to be added slowly in order to oxidize the Mo_2^{4+} complex selectively to a Mo_2^{5+} species. In CH_2Cl_2 solution, $Mo_2(DPhIP)_4$ reacts with $NOBF_4$ (formal potential of $[NO]^+/[NO]$ in CH_2Cl_2 is 1650 mV[11] vs Ag/AgCl) giving a clean reaction and thus an essentially quantitative yield of $Mo_2(DPhIP)_4(BF_4)_2$. The cyclic voltammogram of compound **1** (Figure 3b) shows two quasi-reversible oxidation peaks, implying that both Mo_2^{6+} and Mo_2^{7+} oxidation states are electrochemically accessible, and one complicated irreversible reduction process, implying a possible bond-breaking process. The cyclic voltammogram of **2** (Figure 3b) is very similar to that of the ESBO complex $[PPh_4][Mo_2(DPhF)_2Cl_4]$,[9b] suggesting there are an Mo_2^{7+} accessible species and an irreversible reduction process.

Molecular Structure. The progression from $Mo_2(DPhIP)_4$ to $Mo_2(DPhIP)_4^+$ to $Mo_2(DPhIP)_4^{2+}$ is accompanied by a structural change at each step. In the first one, however, there are only some small quantitative changes, with minimal structural rearrangements as shown in Figure 1.

All that has occurred is the removal of one δ electron, and this causes a slight increase in the Mo−Mo distance from 2.114-(1) to 2.136(2) Å.This small increase results from the offsetting effects of two factors: (1) The loss of the δ electron slightly weakens the Mo−Mo bond by lowering the bond order. (2) Equally important is the increase of positive charge on the metal atoms, which causes a contraction of the entire set of 4d orbitals, thus diminishing the σ and π overlaps. This second factor may also be viewed as an increase in the Coulombic repulsion between the more positive molybdenum atoms. The increase in positive charge on the metal atoms also results in shortening of the Mo−N bonds from an average of 2.166 to 2.148 Å.

Surprisingly, the second oxidation step results in an oxidative scission of the Mo−Mo bond, which is quite different from what occurs in the two-electron oxidation of $Mo_2(hpp)_4$ where a Mo−Mo triple bond with a bond length of 2.142(2) Å was obtained.[7] The product is also different from the known ESBO complexes where the Mo−Mo bonding was still significant (the Mo−Mo distances ranged from 2.4 to 2.7 Å).[9] The molecular structure (Figure 2) of compound **2** shows that each DPhIP ligand uses two of its three nitrogen donor atoms to chelate to one Mo atom, and the third nitrogen atom to coordinate the other Mo atom. The directions of the four DPhIP ligands alternate around the dimolybdenum core; the idealized point group for **2** is D_{2d}. Each Mo atom is in a very distorted octahedral coordination environment with an average N−Mo−N bond angle of 59.7(2)° between the two chelating Mo−N bonds of each ligand. The Mo···Mo distance is 2.9954(7) Å, indicating that there is little or probably no metal−metal bonding.

The type of bioctahedral structure found in **2** has also been observed for V(II) and Cr(III) complexes recently.[12] In all these

(11) Connelly, N. G.; Geiger, W. E. *Chem. Rev.* **1996**, *96*, 877.

(12) Cotton, F. A.; Murillo, C. A.; Zhou, H.-C. Unpublished results.

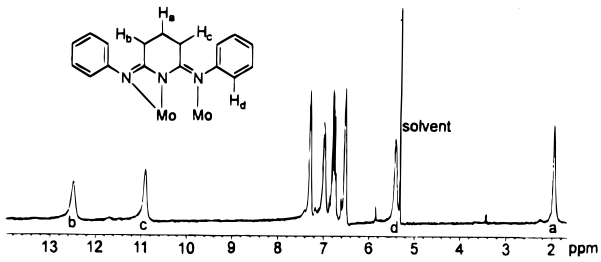

Figure 4. ^{1}H NMR spectrum (in CD_2Cl_2) and assignments of **2** showing the downfield shift and broadening of some of the NMR signals. For simplicity, only one H atom (on each C atom) of the two H_a-H_c atoms of the piperidyl group is shown in the schematic formula insert.

complexes, each metal atom has a d^3 configuration. One might argue that ligand field stabilization energy would play a major role favoring the bioctahedral coordination environment, but other factors could also be important. The bioctahedral ligand arrangement is an extreme case of axial π^* coordination, where the axial coordination is so strong that four M−N bonds have taken over the M−M triple bond, whereas in the $Mo^{2+}-Mo^{2+}$ and $Mo^{2+}-Mo^{3+}$ situations the Mo−Mo bond retention is energetically favored over the formation of four additional M−N bonds; the axial π^* coordination in the $Cr^{2+}-Cr^{2+}$ case[13] implies a balance between metal−metal bonding and metal−ligand bonding.

Both **1** and **2** are expected to be paramagnetic. The ^{1}H NMR spectrum of **1** is too broad to be of value, but the spectrum of **2** shown in Figure 4 is surprisingly well resolved. Several of the lines are quite broad and shifted significantly from the positions where they would normally be expected. Nevertheless, we can make tentative assignments (Figure 4) that are in accord with the structure found in the crystal.

Acknowledgment. We are grateful to the National Science Foundation for financial support.

Supporting Information Available: An X-ray crystallographic file, in CIF format, is available free of charge via the Internet at http://pubs.acs.org.

IC000092T

(13) Cotton, F. A.; Daniels, L. M.; Murillo, C. A.; Pascual, I.; Zhou, H.-C. *J. Am. Chem. Soc.* **1999**, *121*, 6856.